Nitrogen substitution impacts organic-metal interface energetics

Ao Yang,[1] Antoni Franco-Cañellas,[2] Mikio Sato,[3] Bin Wang,[1] Rong-Bin Wang,[1,4] Harunobu Koike,[3] Ingo Salzmann,[4] Pardeep Kumar Thakur,[5] Tien-Lin Lee,[5] Lijia Liu,[1] Satoshi Kera,[6] Alexander Gerlach,[2] Kaname Kanai,[3] Jian Fan,[1] Frank Schreiber,[2] and Steffen Duhm[1,*]

[1]*Institute of Functional Nano and Soft Materials (FUNSOM) and Jiangsu Key Laboratory for Carbon-Based Functional Materials and Devices, Soochow University, Suzhou 215123, PR China*

[2]*Institut für Angewandte Physik, Universität Tübingen, 72076 Tübingen, Germany*

[3]*Department of Physics, Faculty of Science and Technology, Tokyo University of Science, Noda, Chiba 278-8510, Japan*

[4]*Institut für Physik, Humboldt-Universität zu Berlin, 12489 Berlin, Germany*

[5]*Diamond Light Source, Harwell Science and Innovation Campus, Oxfordshire OX11 0DE, United Kingdom*

[6]*Department of Photo-Molecular Science, Institute for Molecular Science, Okazaki, Aichii 444-8585, Japan*

(Received 31 May 2016; published 17 October 2016)

We investigated the structural and electronic properties of vacuum sublimed 7,8,15,16-tetraazaterrylene (TAT) thin films on Au(111), Ag(111), and Cu(111) substrates using inverse photoemission spectroscopy, ultraviolet photoelectron spectroscopy (UPS), x-ray photoelectron spectroscopy (XPS), low energy electron diffraction (LEED), and the x-ray standing wave (XSW) technique. The LEED reveals a flat adsorption geometry of the monolayer TAT on these three substrates, which is in accordance with the XSW results. The molecules are slightly distorted in monolayers on all three substrates with the nitrogen atoms having smaller averaged bonding distances than the carbon atoms. On Ag(111) and Cu(111), chemisorption with a net electron transfer from the substrate to the adsorbate takes place, as evidenced by UPS and XPS. Combining these results, we gain full insight into the correlation between electronic properties and interface geometry.

DOI: 10.1103/PhysRevB.94.155426

I. INTRODUCTION

Substantial effort has been devoted into investigating the contact formation between organic semiconductors (OSCs) and metals over the past decades due to the impact of the energy level-alignment (ELA) on charge-carrier injection efficiencies [1–3]. Only recently, the crucial role of gap states and the density of states (DOS) of frontier molecular orbitals in the ELA have been identified [4–7]. It has been shown that for typical inorganic-organic and organic-organic interfaces, the ELA can be well modeled by approximating the frontier molecular-orbital DOS by Gaussian functions, while the substrate-adsorbate coupling can be taken into account by Lorentzian contributions [6,8,9]. However, at organic/metal interfaces where strong coupling and hybridization between substrate and adsorbate occurs, the successful prediction of the ELA requires an advanced level of calculation [10–13]. Going beyond the contact layer, the packing within organic thin films determines transfer integrals and, thus, charge carrier mobilities [14,15]. In this context, for *rodlike* OSCs forming thin films on various substrates, herringbone motifs are commonly observed [16], whereas π-stacked growth dominates for *disclike* OSCs [16,17]. Such columnar growth usually leads to larger transfer integrals [18,19] and is, thus, favored for efficient charge transport layers.

Many rylene derivatives exhibit excellent thermal and oxidative stability, as well as high electron mobilities in thin films, and, therefore, are employed in a variety of organic electronics applications [20–23]. In this context, the nitrogen-substituted terrylene analogue 7,8,15,16-tetraazaterrylene (TAT; chemical structure in Fig. 1) [24] exhibiting four doubly bonded nitrogen atoms in its molecular structure is a particularly interesting compound as it forms a closely π-stacked single crystal structure [24] and grows in vertically π-stacked nano-rods on graphene substrates [25]. These features render TAT a promising candidate as acceptor material in organic photovoltaic cells (OPVCs). However, in contrast to these well-established bulk properties, the chemical and structural properties of its interface with metals have not yet been explored in detail. The (111)-surfaces of the coinage metals Au, Ag, and Cu cover a wide range of reactivity and, therefore, emerged as model systems to study the contact formation with OSCs such as pentacene [26–29], perylene [30–32], coronene [33–36], diindenoperylene (DIP) [37–40], perylene-3,4,9,10-tetracarboxylic dianhydride (PTCDA) [35,41–44], or 6,13-pentacenequinone (P2O) and 5,7,12,14-pentacenetetrone (P4O) [45–47]. In the present paper, we performed a systematic study of the ELA and molecular surface structure of TAT adsorbed on Au(111), Ag(111), and Cu(111) by combining inverse photoelectron spectroscopy (IPES), ultraviolet photoelectron spectroscopy (UPS), and x-ray photoelectron spectroscopy (XPS) with low energy electron diffraction (LEED) and the x-ray standing wave (XSW) technique.

II. EXPERIMENTAL DETAILS

The UPS, XPS, and LEED experiments were carried out in an ultrahigh vacuum (UHV) system [27] consisting of three interconnected chambers: evaporation chamber (base pressure: 3×10^{-10} mbar), annealing and sputtering chamber (3×10^{-10} mbar), and analysis chamber (base pressure: 2×10^{-10} mbar). The Au(111), Ag(111), and Cu(111) substrates were cleaned by several cycles of Ar^+ ion bombardment and annealing (650–700 K) until XPS showed no traces of contaminants, angle-resolved UPS revealed a clear surface

*duhm@suda.edu.cn

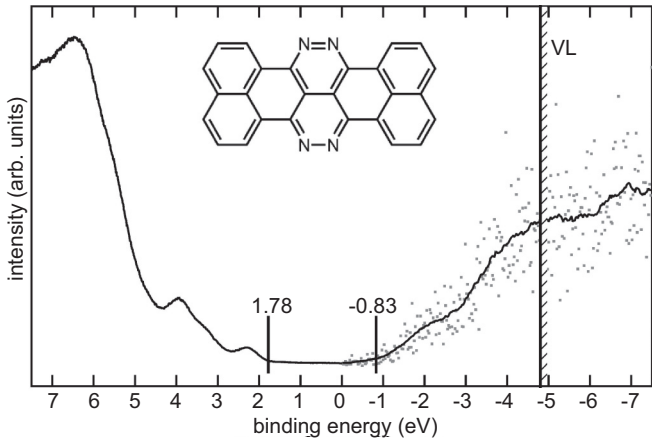

FIG. 1. Composite UPS/IPES spectrum of a nominally 128 Å thick TAT film on Au. The energy scale is relative to the position of the Fermi level E_F, as measured for the Au substrate. The onset of emission from the HOMO and LUMO levels are indicated by vertical lines. The vacuum level (VL) is found at 4.87 eV above E_F.

state, and LEED presented the expected pattern. TAT was synthesized according to Ref. [24] and sublimated *in situ* onto the single crystal surface by physical vapor deposition from home-built, resistively heated Knudsen-cells at room temperature with deposition rates of about 2–3 Å/min. The nominal film mass thickness was monitored with a quartz-crystal microbalance positioned near the samples within the deposition chamber. The LEED experiments were performed using a Micro-Channel-Plate LEED (OCI BDL800IR-MCP). The UPS experiments were performed using monochromatized He I radiation (21.22 eV) and a Specs PHOIBOS 150 analyzer. The energy resolution was set to 80 meV. The angle between the incident beam and the sample was fixed to 40°. The spectra were collected at photoelectron take-off angles (θ) of 45° with an acceptance angle of ±12° along the Γ-M direction of the substrate. The secondary electron cutoff (SECO) [for determination of the sample work function (ϕ) and the ionization energy] was measured in normal emission with a bias potential of −3 V. The XPS was completed using a monochromatized Al K_α source (1486.6 eV). Data analysis was carried out by a nonlinear least-squares fitting routine, using Gaussian/Lorentzian peak shapes (typically 0.9/0.1) and a Shirley background. The error of binding energy (BE) values in UPS is estimated to be ±0.05 eV.

Additional UPS of TAT on highly ordered pyrolytic graphite (HOPG) was measured at the endstation SurICat [48] (beamline PM4) at the synchrotron light source BESSY II (at Helmholtz-Zentrum Berlin) with a photon energy of 35 eV.

The IPES spectra were measured in bremsstrahlung isochromat spectroscopy mode with a band pass energy of 9.5 eV (PSP Vacuum Technology Ltd.), and complementary UPS spectra were measured by using HeI radiation [49]. The energy resolution of IPES was 0.4 eV and 0.1 eV for UPS, as was deduced from the Fermi edge of an Au film.

The XSW experiments were performed at beamline I09 [50] of the Diamond Light Source (DLS). The analysis chamber (base pressure, 3×10^{-10} mbar) contains a VG Scienta EW4000 HAXPES hemispherical electron analyzer, which is mounted at ∼90° relative to the incident x-ray beam. Sample preparation and measurements took place *in situ* under UHV conditions. A typical nominal deposition rate was ∼0.2 Å/min. The final molecular coverage was in the submonolayer range. For the XSW measurements, the photon energy was scanned around the first-order Bragg reflection of the (111) substrates.

All measurements have been performed at room temperature.

III. EXPERIMENTAL RESULTS

A. IPES

The IPES measurements of organic thin films are indispensable in getting reliable transport gaps, which are smaller than the optical gap due to the relatively large exciton binding energy of OSCs [51,52]. From the combined IPES and UPS spectra of a 128 Å TAT film on Au (Fig. 1), the transport gap [as measured by the energetic difference between the onsets of the highest occupied molecular orbital (HOMO) and lowest unoccupied molecular orbital (LUMO)] can be determined to 2.66 eV. TAT thin films have an optical gap of ∼1.98 eV [24], and the exciton binding energy (difference between the transport gap and optical gap) is thus 0.63 eV, which is in the range of exciton binding energies for related OSCs [51]. The energetic difference between the LUMO-onset and the vacuum level gives the solid state electron affinity (EA), which is 4.05 eV for TAT on Au. The solution value for TAT, as measured by cyclic voltammetry, is 3.50 eV [24], and the difference can mainly be ascribed to polarization effects [53,54].

B. LEED

In single crystals, TAT exhibits a π-stacked intermolecular arrangement, and, likewise, a similar packing motif was found for TAT on graphene with the molecules flat lying on the substrate and the stacking direction thus being perpendicular to the sample surface [25]. The possible two-dimensional (2D) surface unit cells, as determined by LEED (Fig. 2) of both TAT mono- (nominal coverage: 4 Å) and multilayer (nominally 128 Å) on Au(111), are orthogonal with the unit-cell parameters similar to those of the (ab)-plane of the TAT single crystal (Table I). (Here the c axis points in the π-stacking direction, which is different from the unit-cell definition in Ref. [24].) Therefore, we conclude that TAT also lies essentially flat on the Au(111) substrate and exhibits π-stacking in the multilayer. On Ag(111), the LEED patterns are highly similar for both coverages (Fig. 2 and Table I). On Cu(111), however, no clear spots could be observed for nominal monolayer coverage; the spots for multilayer coverage are blurred, and no precise surface unit-cell parameters can be determined, although a rough estimation yields intermolecular distances typical for lying molecules. We note that further evidence for lying molecules at the interface to Cu(111) comes from our XSW measurements (see below).

C. UPS

Already the evolution of the vacuum-level position with increasing film coverage (Fig. 3) provides a first insight into the interfacial interaction strength at the organic/metal interface

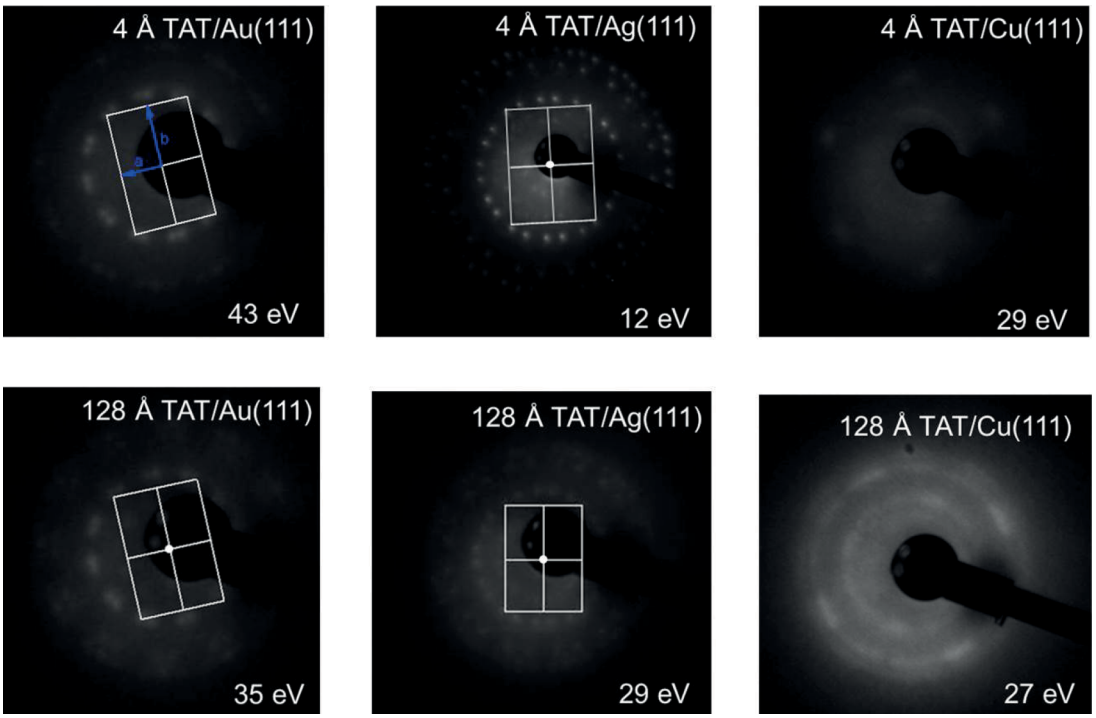

FIG. 2. The LEED images of TAT thin films on Au(111), Ag(111), and Cu(111) for nominal monolayer (4 Å) and multilayer (128 Å) coverage. In each image, the respective electron beam energy is given. On Au(111) and Ag(111), possible surface Brillouin zones are shown; for unit-cell parameters, see Table I.

and the morphology of the thin film [2,55,56]. For all three substrates, the vacuum level shows a steep decrease upon initial TAT deposition, which almost saturates at a nominal coverage of 4 Å and stays essentially constant for all coverages higher than 8 Å. Such behavior points to almost flat lying molecules with a (closed) monolayer formed for a coverage of ∼4 Å and subsequent multilayer growth. On Au(111) ($\phi_{Au} = 5.51$ eV), the total vacuum-level shift is 0.72 eV and is tentatively ascribed to the electron push-back effect [2,57], which is often the main reason for vacuum-level shifts (in the range of up to 1 eV) upon the deposition of OSCs on weakly interacting surfaces such as Au(111) [56]. For Ag(111), the sample work function of the pristine substrate ($\phi_{Ag} = 4.60$ eV) is reduced by 0.31 eV through TAT deposition. Such a relatively small vacuum-level shift, as compared to the Au(111) case, indicates a net electron transfer from the metal to the molecule, which counteracts the push-back effect [58,59]. The work function of the clean Cu(111) substrate is 4.91 eV and decreases by 0.79 eV during subsequent TAT deposition. In this case, the information on the vacuum level alone does not allow drawing unequivocal conclusions on the adsorption behavior. However, a close look at the valence electron region indicates charge transfer between the adsorbate and the Cu(111) substrate (see below).

In the valence-electron region, the deposition of TAT on Au(111) attenuates the Au-derived photoemission features [Fermi-edge, *d* bands in the BE range of ∼2 to ∼8 eV], and a peak centered at 1.35 eV BE arises [Figs. 4(a) and 4(b)], which

TABLE I. Comparison of lattice parameters (in Å) of rectangular TAT surface unit cells on Au(111) and Ag(111) in monolayers (nominally 4 Å coverage) and multilayers (nominally 128 Å coverage), as deduced from LEED. For comparison, the corresponding plane of the TAT single crystal is given; its additional (monoclinic) lattice parameters are $c = 3.7429$ Å (the π-stacking direction) and $\beta = 93.947°$.

	Au(111)		Ag(111)		
	Mono	Multi	Mono	Multi	Single Crystal [24]
a	13.4	13.6	14.1	15.0	13.990
b	16.4	20.4	14.1	21.3	15.815

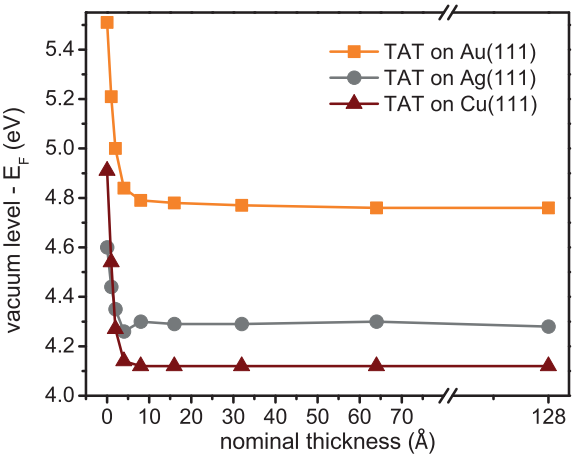

FIG. 3. Vacuum levels of TAT thin films with respect to the substrate Fermi-level (E_F) as a function of nominal TAT coverage; data for 0 Å nominal thickness correspond to the work function of the respective clean metal substrate.

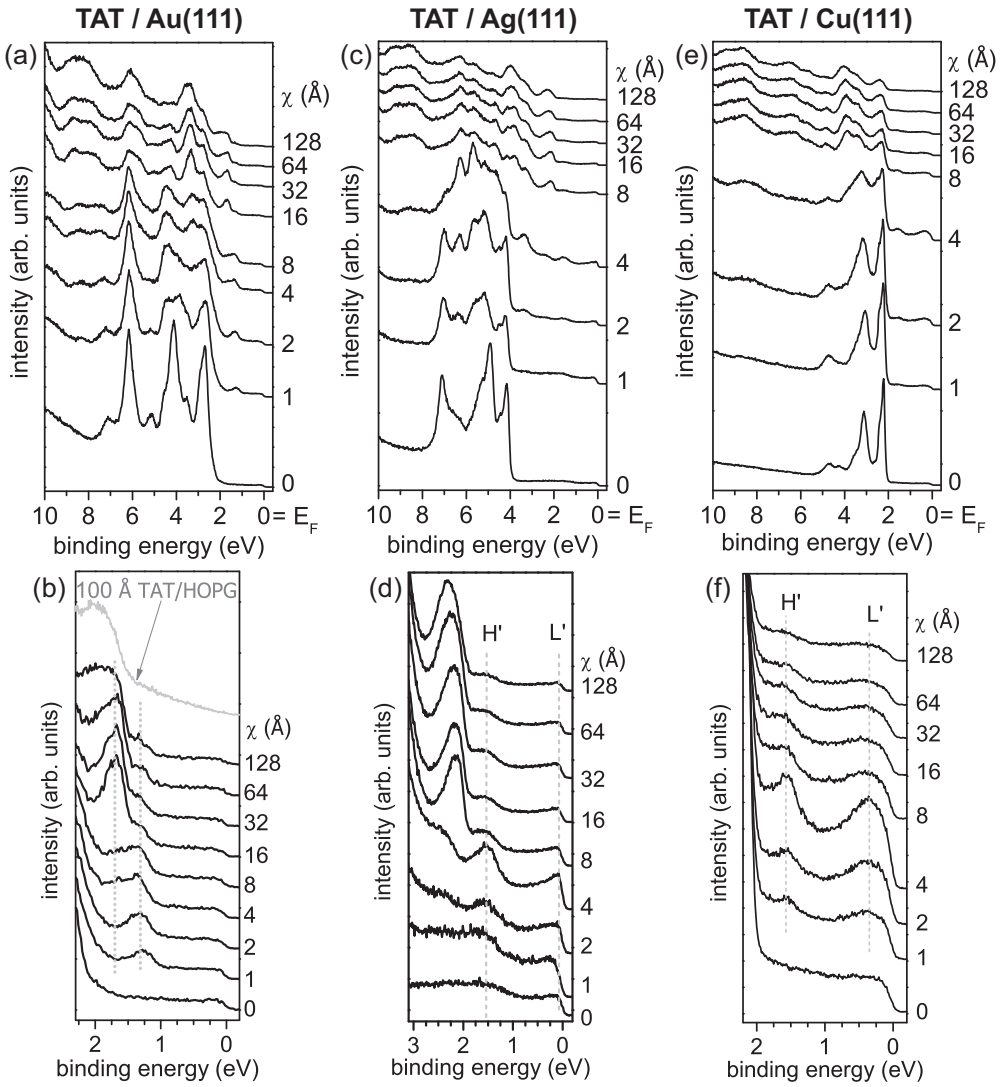

FIG. 4. Thickness-dependent UPS HeI spectra of TAT on Au(111), Ag(111), and Cu(111); χ denotes the layer thickness. The first row shows overview spectra, and the second row shows the corresponding zoom in the region close to the Fermi energy (E_F). The lines are guides to the eye.

is tentatively assigned to be derived from the HOMO of TAT. This peak corresponds to a hole injection barrier (HIB), defined as the energy difference between the low-BE HOMO onset and the Fermi level, of 1.09 eV for a nominal coverage of 4 Å. For this coverage, a further peak centered at 1.70 eV BE emerges, which increases in intensity with the coverage and is, thus, assigned the HOMO emission of TAT in multilayers, which appears at higher BE due to reduced photo-hole screening [2,56]. The HIB of multilayer TAT on Au(111) is 1.44 eV and similar to that of multilayer TAT on HOPG [Fig. 4(b)].

Likewise, new photoemission features arise for the case of 1 Å TAT deposited on Ag(111) [Figs. 4(c) and 4(d)]. A peak centered at 0.08 eV BE appears close to the Fermi edge of the metal substrate (L'), and another peak emerges with its center at 1.67 eV BE (H'). Here, increasing the coverage to 4 Å leads to enhanced intensity of both peaks. For higher coverages, their intensity decreases, and a new peak centered at 2.15 eV BE emerges. We assign L' to be derived from the LUMO of TAT, which is partially occupied by electrons transferred from the substrate. As L' is cut by the Fermi level, the monolayer TAT film on Ag(111) is metallic, as it was found before for various OSC monolayers on metals [45,60]. The feature H' shows the same trend of first gaining and then losing intensity with increasing coverage. Thus, it can be assigned to the relaxed HOMO state of charged molecules. The peak emerging at 2.15 eV BE at a coverage of 8 Å is interpreted as derived from the HOMO of the neutral molecules in multilayers.

Finally, the deposition of 1 Å TAT on Cu(111) [Figs. 4(e) and 4(f)] leads to two photoemission features in the region close to E_F, that is, a broad peak centered at 0.37 eV BE (L') and a peak at 1.53 eV BE (H'). At higher coverages, the intensities of these peaks first increase up to a maximum for 4 Å and then gradually decrease. In analogy to TAT on Ag(111), we assign these features to partially filled former LUMO and the relaxed HOMO of TAT in the monolayer on Cu(111), respectively. The photoemission from the HOMO of neutral TAT in multilayers (onset at 1.93 eV BE) is

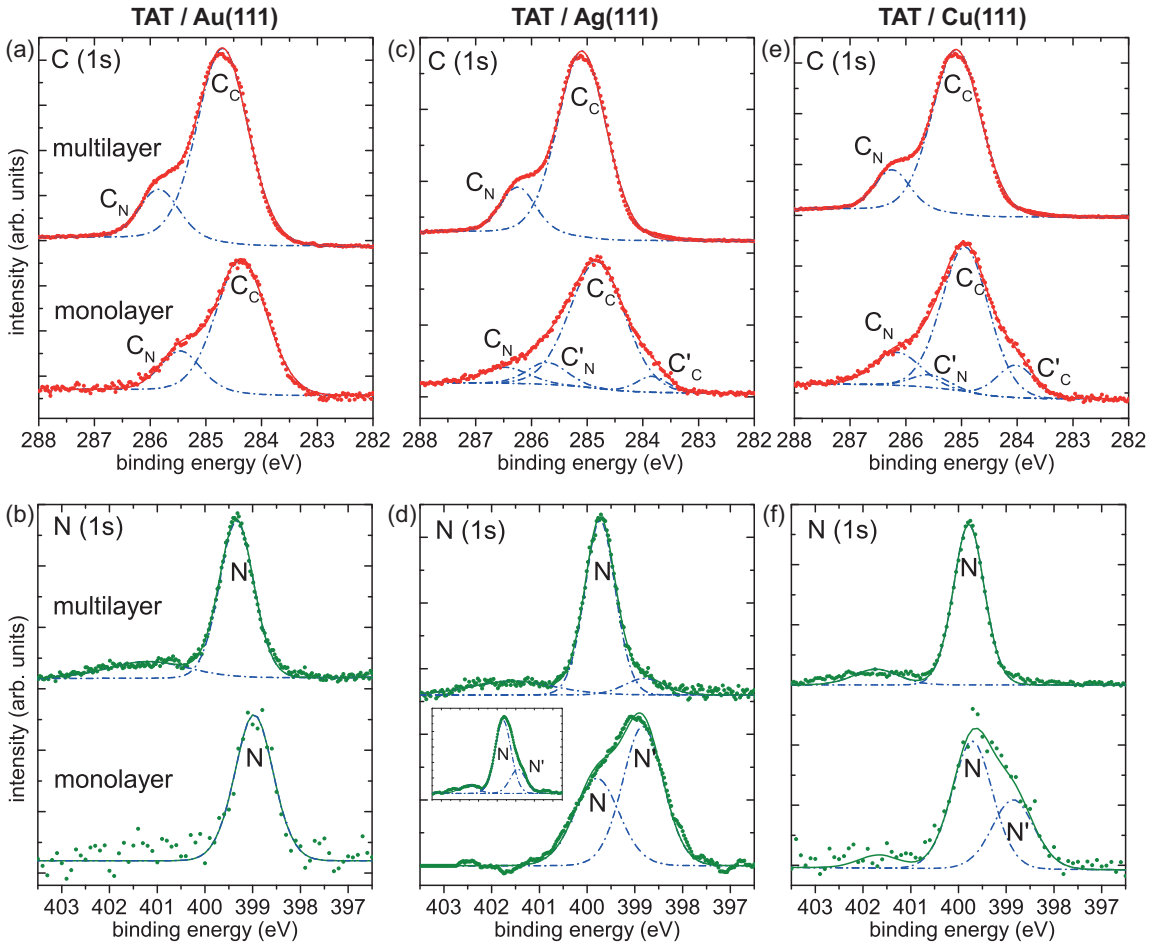

FIG. 5. The XPS spectra of monolayer (nominally 4 Å coverage) and multilayer (nominally 128 Å coverage) TAT on Au(111), Ag(111), and Cu(111) substrates. The inset in (d) shows the N1*s* spectrum for a nominal coverage of 8 Å TAT on Ag(111).

masked here by the pronounced emission of the Cu *d* bands and becomes clearly visible only for a nominal coverage of 128 Å.

D. XPS

The XPS fine structures are very sensitive to subtle differences in interface and bonding situation [60,61]. As shown in Fig. 5(a), the C1*s* signal of monolayer TAT/Au(111) consists of two components (marked by two blue dashed curves) apart from the Shirley background (not shown). The main component (C_C) at a BE of 284.3 eV is related to carbon atoms bound only to carbon or to carbon and hydrogen, while the weaker feature (C_N) at a higher BE of 285.5 eV originates from carbon atoms bound to nitrogen. The observed intensity ratio is 4.7:1, which is in good agreement with the stoichiometric ratio of 5.5:1. The four nitrogen atoms of TAT are chemically equivalent, and the N1*s* peak is centered at 398.9 eV BE for monolayer TAT/Au(111) [Fig. 5(b)]. In the multilayer regime, the peak shifts to 399.3 eV BE, and a second peak at 401.2 eV BE becomes visible, which is ascribed to a shake-up excitation [62,63]. The C1*s* multilayer peak shifts by ∼0.3 eV to higher BEs compared to the monolayer. Thus, the core levels shift almost rigidly with the features in the valence electron region, which clearly supports the initial notion of physisorption on Au(111).

For TAT/Ag(111) in the C1*s* spectrum of the monolayer [Fig. 5(c)], an additional feature (C'_C) appears in the right shoulder of the main component C_C (centered at 284.8 eV BE) with its peak center lower by 1.0 eV. Moreover, in addition to the C_N feature (centered at 286.5 eV BE), a fourth contribution (C'_N) is needed for fitting the spectrum. In contrast, the multilayer TAT/Ag(111) spectrum shows only two contributions centered at 286.2 eV BE (C_N) and 285.1 eV BE (C_C), respectively. As shown in Fig. 5(d), the N1*s* spectrum of monolayer TAT/Ag(111) reveals two components N and N', centered at BEs of 399.8 eV and 398.8 eV, respectively, with peak N' having a larger peak area. In the bilayer regime [inset of Fig. 5(d)], the relative intensity ratio of N and N' changes dramatically compared to that of monolayer. For multilayer TAT/Ag(111), we find a dominant peak centered at 399.7 eV BE, a weaker feature in its right shoulder at 398.8 eV BE and, again, a shake-up excitation. Here, the main features are tentatively assigned to negatively charged TAT in the contact layer with the Ag(111) substrate.

Finally, for TAT/ Cu(111), the monolayer XPS C1*s* spectrum [Fig. 5(e)] shows four peaks: C_N at 286.1 eV BE, C'_N at 285.5 eV BE, C_C at 284.9 eV BE, and C'_C at 283.8 eV BE. In

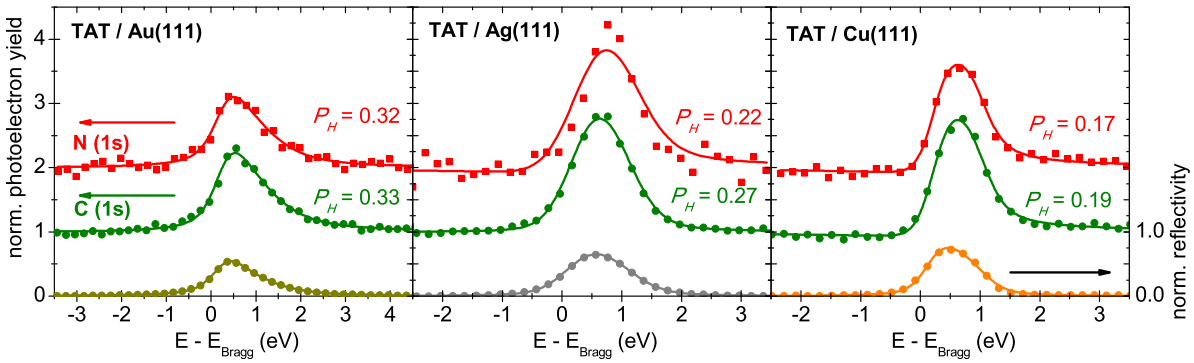

FIG. 6. XSW measurements for TAT submonolayers deposited on the three coinage metals. The normalized photoelectron yield and reflectivity are plotted as a function of the photon energy relative to the respective substrate Bragg energy (E_{Bragg}). The photoelectron yield was calculated adding the areas of the separate components used to fit the monolayer XPS spectra.

the N1*s* spectra [Fig. 5(f)] of TAT/Cu(111), two components are observed in the monolayer spectrum, that is, a feature (N) at 399.7 eV BE and one (N') at 398.8 eV BE. Apart from a shake-up excitation, only one component is found in the multilayer spectrum centered at 399.7 eV BE.

E. XSW

The ELA at organic-metal interfaces is closely related to element-specific vertical bonding distances [1,64,65]. XSW measurements [66,67] of organic monolayers on single-crystalline metal substrates can access vertical adsorption distances with high precision [68]. The core result of the XSW analysis is given by two fitting parameters, that is, the coherent position P_H and the coherent fraction f_H. The first can be simply related to the bonding distance d_H via $d_H = (n + P_H)d_0$. Here, d_0 is the lattice plane spacing of the (111) Bragg reflection, and n is a nonnegative integer. The latter varies within the range of $0 \leqslant f_H \leqslant 1$ and reflects the degree of vertical order.

The photoelectron yields as function of the photon energy of TAT submonolayers on the three investigated (111)-surfaces are displayed in Fig. 6. The coherent fractions for both carbon and nitrogen atoms on all surfaces are around 0.5 (Table II), which points to a rather flat adsorption geometry with a moderate degree of vertical order [64,68]. The averaged adsorption distances of the carbon atoms decrease from 3.06 Å on Au(111) over 2.99 Å on Ag(111) to 2.48 Å on Cu(111). These values are similar to that of DIP on the same surfaces [37], and, likewise, the trend is the same for PTCDA [69–71]. In all cases, the averaged bonding distance of the nitrogen atoms is only slightly below (0.02 to 0.11 Å) that of the carbons. Note that this is in contrast to PTCDA, where chemisorption on Ag(111) and Cu(111) leads to strong molecular distortions (up to 0.30 Å difference between oxygen and carbon atoms) [69,70].

IV. DISCUSSION

The results of the present paper are schematically summarized in Fig. 7. The electronic structure of TAT monolayers strongly depends on the substrate nature: The LUMO-derived feature in the monolayer is well pronounced and well below the Fermi level on Cu(111), weaker and closer to E_F on Ag(111), and not observed on Au(111). This indicates that the degree of electron transfer from the substrate into the former LUMO is strongest on Cu(111). As a consequence, such a directed charge transfer leads to an interface dipole, which *in*creases the vacuum level. However, for TAT on Cu(111), the vacuum level *de*creases (by 0.79 eV). This can be related to pronounced charge rearrangement across organic/metal interfaces upon chemisorption, which can include also back donation involving deeper lying orbitals [72–76]. In this context, site-specific interactions [76–78] are of special interest, and a closer inspection of the XPS data reveals that these interactions are different on Ag(111) and Cu(111). For monolayer TAT on Ag(111), the peak area of feature N' (stemming from charged TAT) is almost twice as large as that of feature N (due to neutral TAT), and the area of C'_N is slightly larger than that of C_N [Figs. 5(c) and 5(d)]. The area of C'_C, however, is almost negligible compared to C_C. This points to a localization of the transferred charge at the vicinity of nitrogen atoms of TAT. This is supported by the distortion of TAT on Ag(111), which here is the largest of all three investigated substrates (0.11 Å difference in the averaged bonding distances of carbon and nitrogen atoms). On Cu(111), the differences in the intensity

TABLE II. Coherent fraction (f_H), coherent position (P_H), and averaged bonding distances (d_H) of TAT submonolayers on coinage metal surfaces. For the bonding distances on Au(111), the surface reconstruction, which decreases the actual adsorption distance from the measured values (for carbon 3.13 Å and for nitrogen 3.11 Å), is taken into account [71].

	Carbon			Nitrogen		
Substrate	f_H	P_H	d_H(Å)	f_H	P_H	d_H(Å)
Au(111)	0.39	0.33	3.06 ± 0.07	0.30	0.32	3.04 ± 0.02
Ag(111)	0.65	0.27	2.99 ± 0.05	0.92[a]	0.22	2.88 ± 0.10
Cu(111)	0.53	0.19	2.48 ± 0.04	0.46	0.17	2.44 ± 0.06

[a]Due to a rather low signal-to-noise ratio for the nitrogen N1*s* signal, the decoupling of it from the overlapping Ag3*d* plasmon was not straightforward. Thus, the given coherent fraction might not be as high as the fit shows. However, and due to the molecule geometry, it is not expected to be lower than that of carbon.

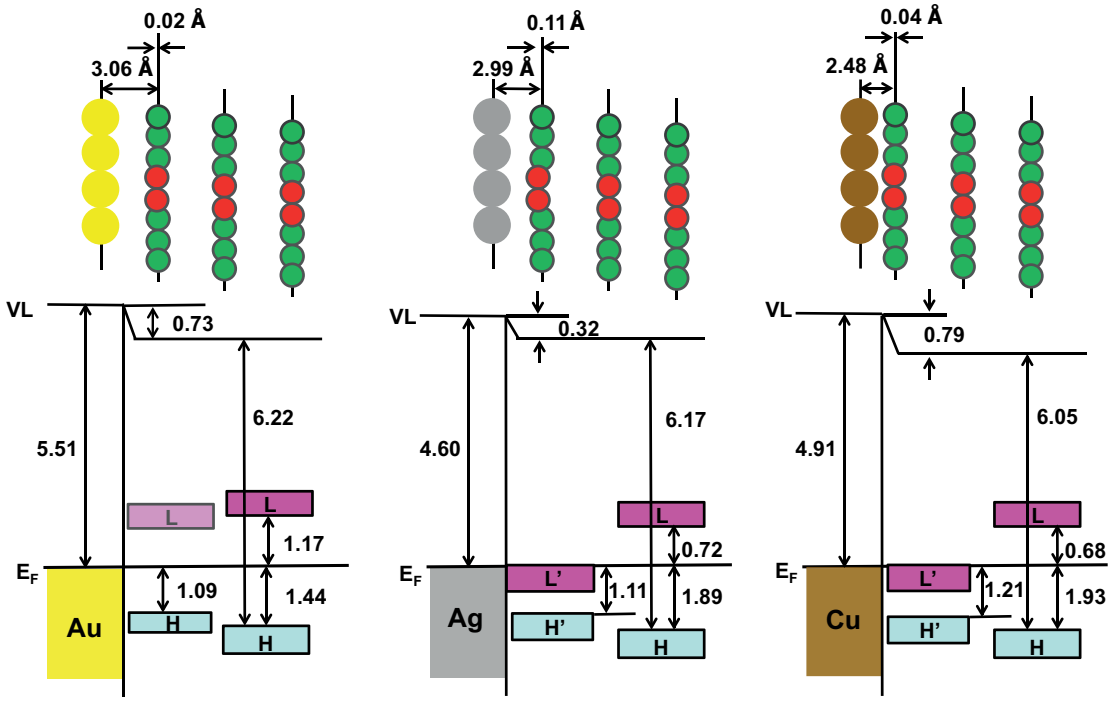

FIG. 7. Schematics of structure and electronic structure at the interface between TAT and Au(111), Ag(111), and Cu(111). The averaged bonding distances of the monolayers stem from XSW, π-stacked multilayer growth is deduced from LEED. The energy positions of the HOMO (H), the relaxed HOMO (H'), and the partially filled former LUMO (L') were deduced from UPS. The position of the LUMO (L) is estimated by the transport gap, which was derived from the combined UPS and IPES data.

ratios of N/N' and C_C/C'_C are less pronounced [Figs. 5(e) and 5(f)], which goes along with a less pronounced distortion of the molecule.

The packing structure of TAT on Au(111) and Ag(111) is rather similar for both the mono- and the multilayer case. However, the position of the Fermi level in the gap (and, thus, also the HIB) differs by 0.45 eV for multilayers, although one might expect an identical E_F position for isostructural cases [9,79–81], as observed for TAT multilayers on Au(111) and HOPG [Fig. 4(b)]. However, the strong coupling at the Ag(111)/TAT interface pulls down the energy levels such that the same HIB cannot be practically reached on the film-thickness scale explored in this paper (nominally up to 128 Å). Interestingly, despite the significantly different interfacial coupling and the different packing structure of TAT on Ag(111) and Cu(111), the multilayer HIBs are identical within the error margin. This can be explained by a three-layer ELA model, as suggested for PTCDA [41], which involves, in particular, a chemisorbed monolayer. The absence of such a layer on Au(111) then rationalizes the more midgap position of E_F. Moreover, although the TAT multilayer HIBs are similar on Ag(111) and Cu(111), the respective ionization energies are different. This can be explained by the different structure and points to slightly tilted TAT molecules on Cu(111), which leads to an increased ionization energy [82].

V. CONCLUSION

Our paper reveals that for thin films of TAT, the molecular packing does not critically depend on the substrate properties. On all investigated substrates, the molecules adopt a flat-lying orientation in the monolayer regime, and on both Au(111) and Ag(111), TAT exhibits π-stacking in the multilayer, which is expected to be favorable for charge transport perpendicular to the substrate surface. On Au(111), TAT is physisorbed, leading to an almost midgap position of the Fermi level for multilayer films. Counterintuitively, the chemical interaction of TAT with the Ag(111) and Cu(111) substrates leading to the partial filling of the former LUMO results in *deeper* lying HOMOs in TAT multilayers on these substrates.

ACKNOWLEDGMENTS

We thank Diamond Light Source for access to beamline I09 (Proposal No. SI 9523-1) and Helmholtz-Zentrum Berlin for access to beamline PM4 at BESSY II, which contributed to the results presented here. Financial support from the Major State Basic Research Development Program of China (973 Program No. 2013CB933500 and No. 2014CB932600), Jiangsu province technology (Grant No. BK20141188), a National Natural Science Foundation of China (NSFC) Research Fund for International Young Scientists (No. 11550110176), a joint Japan Society for the Promotion of Science (JSPS)-NSFC project (Grant No. 612111116), the NSFC (Grant No. 21472135), the Natural Science Foundation of Jiangsu Province of China (BK20151216) the Deutsche Forschungsgemeinschaft (DFG) (in particular Project FoMEDOS, Project No. 624765), the Soochow University-Western University Center for Synchrotron Radiation Research, and the Collaborative Innovation Center of Suzhou Nano Science and Technology (NANO-CIC) are gratefully acknowledged.

A.Y. and A.F.-C. contributed equally to this work.

[1] E. Goiri, P. Borghetti, A. El-Sayed, J. E. Ortega, and D. G. de Oteyza, Adv. Mater. **28**, 1340 (2016).

[2] A. Kahn, N. Koch, and W. Gao, J. Polym. Sci., Part B: Polym. Phys. **41**, 2529 (2003).

[3] *The Molecule-Metal Interface*, edited by N. Koch, N. Ueno, and A. T. S. Wee (Wiley-VCH, Weinheim, 2013).

[4] F. Bussolotti, S. Kera, K. Kudo, A. Kahn, and N. Ueno, Phys. Rev. Lett. **110**, 267602 (2013).

[5] G. Horowitz, J. Appl. Phys. **118**, 115502 (2015).

[6] M. Oehzelt, K. Akaike, N. Koch, and G. Heimel, Sci. Adv. **1**, e1501127 (2015).

[7] S. Yogev, R. Matsubara, M. Nakamura, U. Zschieschang, H. Klauk, and Y. Rosenwaks, Phys. Rev. Lett. **110**, 036803 (2013).

[8] L. Ley, Y. Smets, C. I. Pakes, and J. Ristein, Adv. Funct. Mater. **23**, 794 (2013).

[9] M. Oehzelt, N. Koch, and G. Heimel, Nat. Commun. **5**, 4174 (2014).

[10] D. A. Egger, Z. F. Liu, J. B. Neaton, and L. Kronik, Nano Lett. **15**, 2448 (2015).

[11] Y. L. Huang, E. Wruss, D. A. Egger, S. Kera, N. Ueno, W. A. Saidi, T. Bucko, A. T. Wee, and E. Zojer, Molecules **19**, 2969 (2014).

[12] W. Liu, A. Tkatchenko, and M. Scheffler, Acc. Chem. Res. **47**, 3369 (2014).

[13] S. Yanagisawa, K. Okuma, T. Inaoka, and I. Hamada, J. Electron. Spectrosc. Relat. Phenom. **204**, 159 (2015).

[14] X. Feng, V. Marcon, W. Pisula, M. R. Hansen, J. Kirkpatrick, F. Grozema, D. Andrienko, K. Kremer, and K. Müllen, Nat. Mater. **8**, 421 (2009).

[15] Z. Shuai, H. Geng, W. Xu, Y. Liao, and J. M. Andre, Chem. Soc. Rev. **43**, 2662 (2014).

[16] A. O. F. Jones, B. Chattopadhyay, Y. H. Geerts, and R. Resel, Adv. Funct. Mater. **26**, 2233 (2016).

[17] X. Feng, W. Pisula, and K. Müllen, Pure. Appl. Chem. **81**, 2203 (2009).

[18] V. Coropceanu, J. Cornil, D. A. da Silva Filho, Y. Olivier, R. Silbey, and J.-L. Brédas, Chem. Rev. **107**, 926 (2007).

[19] I. Salzmann, A. Moser, M. Oehzelt, T. Breuer, X. Feng, Z. Y. Juang, D. Nabok, R. G. Della Valle, S. Duhm, G. Heimel, A. Brillante, E. Venuti, I. Bilotti, C. Christodoulou, J. Frisch, P. Puschnig, C. Draxl, G. Witte, K. Müllen, and N. Koch, ACS Nano **6**, 10874 (2012).

[20] L. Chen, C. Li, and K. Müllen, J. Mater. Chem. C **2**, 1938 (2014).

[21] V. Kamm, G. Battagliarin, I. A. Howard, W. Pisula, A. Mavrinskiy, C. Li, K. Müllen, and F. Laquai, Adv. Energy. Mater. **1**, 297 (2011).

[22] C. Musumeci, I. Salzmann, S. Bonacchi, C. Röthel, S. Duhm, N. Koch, and P. Samorì, Adv. Funct. Mater. **25**, 2501 (2015).

[23] F. Würthner and M. Stolte, Chem. Commun. **47**, 5109 (2011).

[24] J. Fan, L. Zhang, A. L. Briseno, and F. Wudl, Org. Lett. **14**, 1024 (2012).

[25] A. Wise, Y. Zhang, J. Fan, F. Wudl, A. Briseno, and M. Barnes, Phys. Chem. Chem. Phys. **16**, 15825 (2014).

[26] D. Dougherty, W. Jin, W. Cullen, J. Reutt-Robey, and S. Robey, J. Phys. Chem. Lett. C **112**, 20334 (2008).

[27] M.-C. Lu, R.-B. Wang, A. Yang, and S. Duhm, J. Phys.: Condens. Matter **28**, 094005 (2016).

[28] W.-H. Soe, C. Manzano, A. De Sarkar, N. Chandrasekhar, and C. Joachim, Phys. Rev. Lett. **102**, 176102 (2009).

[29] K. Toyoda, I. Hamada, K. Lee, S. Yanagisawa, and Y. Morikawa, J. Chem. Phys. **132**, 134703 (2010).

[30] L. Ding, P. Schulz, A. Farahzadi, K. V. Shportko, and M. Wuttig, J. Chem. Phys. **136**, 054503 (2012).

[31] K. Manandhar and B. Parkinson, J. Phys. Chem. C **114**, 15394 (2010).

[32] J. T. Sun, L. Gao, X. B. He, Z. H. Cheng, Z. T. Deng, X. Lin, H. Hu, S. X. Du, F. Liu, and H. J. Gao, Phys. Rev. B **83**, 115419 (2011).

[33] S.-Y. Hong, P.-C. Yeh, I. Lee, J. Yu, J. I. Dadap, C. Nuckolls, and R. M. Osgood, J. Phys. Chem. C **118**, 6214 (2014).

[34] P. V. C. Medeiros, G. K. Gueorguiev, and S. Stafström, Carbon **81**, 620 (2015).

[35] F. Sellam, T. Schmitz-Hübsch, M. Toerker, S. Mannsfeld, H. Proehl, T. Fritz, K. Leo, C. Simpson, and K. Müllen, Surf. Sci. **478**, 113 (2001).

[36] M. Wießner, N. S. Rodríguez Lastra, J. Ziroff, F. Forster, P. Puschnig, L. Dössel, K. Müllen, A. Schöll, and F. Reinert, New J. Phys. **14**, 113008 (2012).

[37] C. Bürker, N. Ferri, A. Tkatchenko, A. Gerlach, J. Niederhausen, T. Hosokai, S. Duhm, J. Zegenhagen, N. Koch, and F. Schreiber, Phys. Rev. B **87**, 165443 (2013).

[38] M. B. Casu, B. E. Schuster, I. Biswas, C. Raisch, H. Marchetto, T. Schmidt, and T. Chassé, Adv. Mater. **22**, 3740 (2010).

[39] H. Huang, J. T. Sun, Y. P. Feng, W. Chen, and A. T. Wee, Phys. Chem. Chem. Phys. **13**, 20933 (2011).

[40] K. Yonezawa, Y. Suda, S. Yanagisawa, T. Hosokai, K. Kato, T. Yamaguchi, H. Yoshida, N. Ueno, and S. Kera, Appl. Phys. Express **9**, 045201 (2016).

[41] S. Duhm, A. Gerlach, I. Salzmann, B. Bröker, R. Johnson, F. Schreiber, and N. Koch, Org. Electron. **9**, 111 (2008).

[42] P. Fenter, F. Schreiber, L. Zhou, P. Eisenberger, and S. R. Forrest, Phys. Rev. B **56**, 3046 (1997).

[43] V. G. Ruiz, W. Liu, and A. Tkatchenko, Phys. Rev. B **93**, 035118 (2016).

[44] F. S. Tautz, Prog. Surf. Sci. **82**, 479 (2007).

[45] G. Heimel, S. Duhm, I. Salzmann, A. Gerlach, A. Strozecka, J. Niederhausen, C. Bürker, T. Hosokai, I. Fernandez-Torrente, G. Schulze, S. Winkler, A. Wilke, R. Schlesinger, J. Frisch, B. Bröker, A. Vollmer, B. Detlefs, J. Pflaum, S. Kera, K. J. Franke *et al.*, Nat. Chem. **5**, 187 (2013).

[46] S. Kawai, B. Eren, L. Marot, and E. Meyer, ACS Nano **8**, 5932 (2014).

[47] N. Koch, I. Salzmann, R. L. Johnson, J. Pflaum, R. Friedlein, and J. P. Rabe, Org. Electron. **7**, 537 (2006).

[48] A. Vollmer, O. D. Jurchescu, I. Arfaoui, I. Salzmann, T. T. M. Palstra, P. Rudolf, J. Niemax, J. Pflaum, J. P. Rabe, and N. Koch, Eur. Phys. J. E. **17**, 339 (2005).

[49] M. Sato, A. Tohkairin, K. Mase, and K. Kanai, Org. Electron. **27**, 247 (2015).

[50] C. Bürker, A. Franco-Cañellas, K. Broch, T.-L. Lee, A. Gerlach, and F. Schreiber, J. Phys. Chem. C **118**, 13659 (2014).

[51] P. I. Djurovich, E. I. Mayo, S. R. Forrest, and M. E. Thompson, Org. Electron. **10**, 515 (2009).

[52] S. R. Forrest, Philos. Trans. A: Math. Phys. Eng. Sci. **373**, 20140320 (2015).

[53] W. Han, H. Yoshida, N. Ueno, and S. Kera, Appl. Phys. Lett. **103**, 123303 (2013).

[54] Y. Kang, S. H. Jeon, Y. Cho, and S. Han, Phys. Rev. B **93**, 035131 (2016).
[55] H. Ishii, K. Sugiyama, E. Ito, and K. Seki, Adv. Mater. **11**, 605 (1999).
[56] N. Koch, J. Phys.: Condens. Matter **20**, 184008 (2008).
[57] G. Witte, S. Lukas, P. S. Bagus, and C. Wöll, Appl. Phys. Lett. **87**, 263502 (2005).
[58] N. Koch, S. Duhm, J. P. Rabe, S. Rentenberger, R. L. Johnson, J. Klankermayer, and F. Schreiber, Appl. Phys. Lett. **87**, 101905 (2005).
[59] N. Koch, S. Duhm, J. P. Rabe, A. Vollmer, and R. L. Johnson, Phys. Rev. Lett. **95**, 237601 (2005).
[60] Y. Zou, L. Kilian, A. Schöll, T. Schmidt, R. Fink, and E. Umbach, Surf. Sci. **600**, 1240 (2006).
[61] A. Schöll, Y. Zou, T. Schmidt, R. Fink, and E. Umbach, J. Phys. Chem. B **108**, 14741 (2004).
[62] M. S. Deleuze, A. B. Trofimov, and L. S. Cederbaum, J. Chem. Phys. **115**, 5859 (2001).
[63] E. E. Rennie, B. Kempgens, H. M. Köppe, U. Hergenhahn, J. Feldhaus, B. S. Itchkawitz, A. L. D. Kilcoyne, A. Kivimäki, K. Maier, M. N. Piancastelli, M. Polcik, A. Rüdel, and A. M. Bradshaw, J. Chem. Phys. **113**, 7362 (2000).
[64] S. Duhm, C. Bürker, T. Hosokai, and A. Gerlach, in *Electronic Processes in Organic Electronics,* edited by H. Ishii, K. Kudo, T. Nakayama, and N. Ueno (Springer, Tokyo, 2015), pp. 89–107.
[65] B. Stadtmüller, S. Schröder, and C. Kumpf, J. Electron. Spectrosc. Relat. Phenom. **204**, 80 (2015).
[66] D. P. Woodruff, Rep. Prog. Phys. **68**, 743 (2005).
[67] J. Zegenhagen, Surf. Sci. Rep. **18**, 202 (1993).
[68] A. Gerlach, C. Bürker, T. Hosokai, and F. Schreiber, in *The Molecule-Metal Interface,* edited by N. Koch, N. Ueno, and A. T. S. We (Wiley-VCH, Weinheim, 2013), pp. 153–172.
[69] A. Gerlach, S. Sellner, F. Schreiber, N. Koch, and J. Zegenhagen, Phys. Rev. B **75**, 045401 (2007).
[70] A. Hauschild, K. Karki, B. C. C. Cowie, M. Rohlfing, F. S. Tautz, and M. Sokolowski, Phys. Rev. Lett. **94**, 036106 (2005).
[71] S. K. M. Henze, O. Bauer, T. L. Lee, M. Sokolowski, and F. S. Tautz, Surf. Sci. **601**, 1566 (2007).
[72] D. A. Egger and E. Zojer, J. Phys. Chem. Lett. **4**, 3521 (2013).
[73] L. Romaner, G. Heimel, J. L. Bredas, A. Gerlach, F. Schreiber, R. L. Johnson, J. Zegenhagen, S. Duhm, N. Koch, and E. Zojer, Phys. Rev. Lett. **99**, 256801 (2007).
[74] L. Romaner, D. Nabok, P. Puschnig, E. Zojer, and C. Ambrosch-Draxl, New J. Phys. **11**, 053010 (2009).
[75] T. C. Tseng, C. Urban, Y. Wang, R. Otero, S. L. Tait, M. Alcami, D. Ecija, M. Trelka, J. M. Gallego, N. Lin, M. Konuma, U. Starke, A. Nefedov, A. Langner, C. Wöll, M. A. Herranz, F. Martin, N. Martin, K. Kern, and R. Miranda, Nat. Chem. **2**, 374 (2010).
[76] M. Willenbockel, D. Lüftner, B. Stadtmüller, G. Koller, C. Kumpf, S. Soubatch, P. Puschnig, M. G. Ramsey, and F. S. Tautz, Phys. Chem. Chem. Phys. **17**, 1530 (2015).
[77] J. N. O'Shea, A. Saywell, G. Magnano, L. M. A. Perdigão, C. J. Satterley, P. H. Beton, and V. R. Dhanak, Surf. Sci. **603**, 3094 (2009).
[78] H. Yamane, A. Gerlach, S. Duhm, Y. Tanaka, T. Hosokai, Y. Y. Mi, J. Zegenhagen, N. Koch, K. Seki, and F. Schreiber, Phys. Rev. Lett. **105**, 046103 (2010).
[79] F. Bussolotti, J. Yang, A. Hinderhofer, Y. Huang, W. Chen, S. Kera, A. T. S. Wee, and N. Ueno, Phys. Rev. B **89**, 115319 (2014).
[80] X.-H. Shi, J.-X. Sun, C.-H. Xiong, and L. Sun, Org. Electron. **30**, 60 (2016).
[81] K. Yonezawa, A. Hinderhofer, T. Hosokai, K. Kato, R. Makino, F. Schreiber, N. Ueno, and S. Kera, Adv. Mater. Interfaces **1**, 1400004 (2014).
[82] G. Heimel, I. Salzmann, S. Duhm, and N. Koch, Chem. Mater. **23**, 359 (2011).